
CAT: Contrastive Adversarial Training for Evaluating the Robustness of Protective Perturbations in Latent Diffusion Models

Sen Peng¹ Mingyue Wang¹ Jianfei He¹ Jijia Yang¹ Xiaohua Jia¹

Abstract

Latent diffusion models have recently demonstrated superior capabilities in many downstream image synthesis tasks. However, customization of latent diffusion models using unauthorized data can severely compromise the privacy and intellectual property rights of data owners. Adversarial examples as protective perturbations have been developed to defend against unauthorized data usage by introducing imperceptible noise to customization samples, preventing diffusion models from effectively learning them. In this paper, we first reveal that the primary reason adversarial examples are effective as protective perturbations in latent diffusion models is the distortion of their latent representations, as demonstrated through qualitative and quantitative experiments. We then propose the Contrastive Adversarial Training (CAT) utilizing adapters as an adaptive attack against these protection methods, highlighting their lack of robustness. Extensive experiments demonstrate that our CAT method significantly reduces the effectiveness of protective perturbations in customization configurations, urging the community to reconsider and enhance the robustness of existing protective perturbation methods. Code is available at <https://github.com/senp98/CAT>.

1. Introduction

Diffusion-based image generation models, especially the Latent Diffusion Models (LDMs) (Rombach et al., 2022), have exhibited strong capabilities across various downstream image generation tasks, including text-to-image synthesis (Dhariwal & Nichol, 2021; Rombach et al., 2022), image-to-image translation (Saharia et al., 2022; Zhang et al., 2023), image editing (Kawar et al., 2023), and image inpainting (Lugmayr et al., 2022). By utilizing the open-source LDM such as Stable Diffusion (Stability.ai, 2024) as

the pre-trained model, users can customize image generation models on their datasets at a significantly lower cost than training from scratch. Despite their prominence and popularity, the customization of LDMs also raises significant concerns regarding privacy and Intellectual Property Rights (IPRs) (Dixit, 2023; LLP, 2023). It can be misused to generate fake human face images of a specific identity (Li et al., 2022) or mimic the style of a specific artist by utilizing unauthorized data. Undoubtedly, such malicious customization severely compromises the rights of data owners and raises ethical concerns across the community.

Several protective perturbation methods (Salman et al., 2023; Liang et al., 2023; Shan et al., 2023; Van Le et al., 2023; Liang & Wu, 2023; Xue et al., 2023; Liu et al., 2024) have been proposed to address these concerns in diffusion-based image generation. These methods introduce imperceptible perturbations to image samples in the customization dataset, creating adversarial examples that effectively degrade the performance of downstream task customization. Although significant progress has been made in developing perturbation methods, the robustness of these protection techniques has received limited attention. Recent studies (Zhao et al., 2024; Cao et al., 2024; Hönig et al., 2024) have investigated the resilience of protective perturbations against purification-based adaptive attacks. By purifying the protected images before customization, these methods effectively compromise the robustness of existing protective perturbation. However, existing purification-based adaptive attacks depend on optimization, resulting in high computational costs. Without an efficient mechanism to detect the protected perturbed images, purification must be applied to every sample in the customization dataset, increasing resource demand. Furthermore, purification without prior knowledge of the original data distribution introduces uncertainty, potentially altering the learned distribution. In extreme cases, optimization-based purification may entirely replace the original image content if the substituted one achieves a lower loss for the optimization objective.

In this paper, we introduce Contrastive Adversarial Training (CAT) from a novel perspective, focusing on model adaptation rather than purification as a solution approach. We first reveal that the primary reason adversarial examples are effective as protective perturbations in LDM customization

¹Department of Computer Science, City University of Hong Kong, Kowloon, Hong Kong SAR. Correspondence to: Sen Peng <first1.last1@xxx.edu>.

is that their latent representations are distorted. Building on this insight, we develop the CAT method targeting the latent autoencoder of the LDM, utilizing the contrastive adversarial loss to minimize the reconstruction loss of protected image samples. During adversarial training, we introduce LoRA adapters (Hu et al., 2022) to specific layers of the latent autoencoder, ensuring that only the adapter weights are modified. This approach expands the parameter space to mitigate the effectiveness of adversarial examples and reduces computational costs, enhancing its adaptability across different scenarios. Extensive experiments demonstrate that applying CAT decreases the effectiveness of protective perturbations, urging the community to reconsider their robustness. In summary, our main contributions are as follows:

1. We identify that the primary reason adversarial examples effectively serve as protective perturbations in LDM customization is the distortion of their latent representations.
2. We propose contrastive adversarial training with adapters as an adaptive attack to evaluate the robustness of existing protective perturbation methods from a novel perspective of model adaptation rather than purification.
3. We conduct extensive experiments demonstrating that applying CAT can significantly reduce the effectiveness of existing perturbation methods, urging the community to reconsider their robustness.

2. Related Works

2.1. Diffusion-based Text-to-Image Models

Diffusion-based text-to-image models have demonstrated remarkable capabilities across various downstream tasks. Images are learned through the forward diffusion process, while generation involves denoising in the reverse diffusion process, typically using a U-Net (Ronneberger et al., 2015) as the backbone model (Ho et al., 2020). Latent diffusion models (Rombach et al., 2022) improve training and inference efficiency while maintaining generation quality by encoding samples into their latent space representations through a latent autoencoder before the diffusion process. Stable Diffusion (Stability.ai, 2024) is later released as an open-source LDM, significantly boosting the development of various downstream applications in diffusion-based text-to-image generation.

2.2. Customization of LDMs

Customization of LDMs can be applied to various downstream tasks, which are classified into two categories: text-driven image synthesis and text-driven image editing. Text-driven image synthesis can be divided into (1) object-driven image synthesis and (2) style mimicry. The former generates images of a specific object based on the given text prompt, while the latter generates images that adopt a spe-

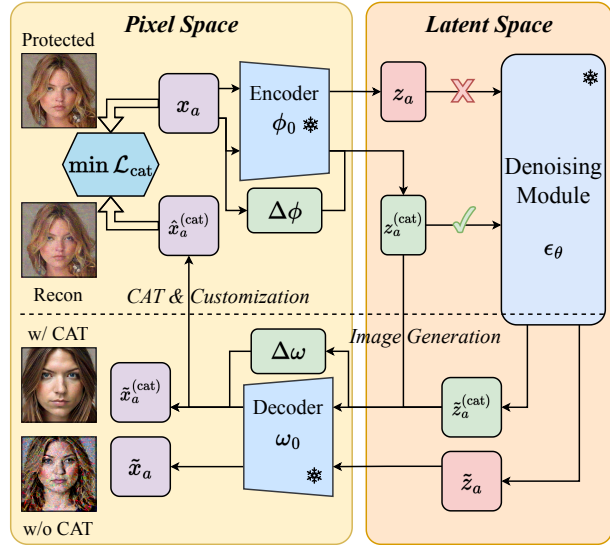


Figure 1. Overview of the proposed CAT method. The CAT adapters ($\Delta\phi$ and $\Delta\omega$) are integrated into the latent encoder and decoder to realign the latent representations of protected samples. Instead of directly using z_a for the denoising module in the diffusion process, the protected image x_a is first encoded into the realigned latent representation $z_a^{(\text{cat})}$ through the adapted encoder, then decoded into $\hat{x}_a^{(\text{cat})}$ using the adapted decoder. This process ensures that the generated image $\hat{x}_a^{(\text{cat})}$ is correctly decoded into the pixel space, effectively neutralizing the protective perturbations.

cific style defined by the text prompt. DreamBooth (Ruiz et al., 2023) customizes text-to-image models by fine-tuning the U-Net and text encoder with a few images and employing a class-specific prior preservation loss, enabling the image generation of the target subject while preserving its key features. LoRA (Hu et al., 2022) was initially proposed to reduce the cost of fine-tuning large language models and later applied to diffusion model customization. It assumes that the model’s weight updates form a low-rank matrix, which can be represented through its rank decomposition. By introducing lightweight adaptation layers to a frozen pre-trained model and updating only these layers during customization, LoRA significantly lowers the computational cost during customization.

2.3. Protective Perturbations

The idea of protective perturbations originates from adversarial attacks (Goodfellow et al., 2014) in classification models, where small perturbations mislead the model into making incorrect predictions. Recent work (Salman et al., 2023; Liang et al., 2023; Shan et al., 2023; Van Le et al., 2023; Liang & Wu, 2023; Xue et al., 2023) shows that diffusion-based generative models are also vulnerable to

such attacks, with adversarial examples serving as protective perturbations that significantly degrade the performance of downstream tasks, preventing unauthorized customization. Photoguard (Salman et al., 2023) first introduced protective perturbations to increase the cost of diffusion-based image editing such as SDEdit (Meng et al., 2021). The perturbation is created by maximizing the latent and diffusion denoising loss over the protected images. Both AdvDM (Liang et al., 2023) and SDS (Xue et al., 2023) generate perturbations targeting the entire LDM through end-to-end optimization to prevent learning, while Glaze (Shan et al., 2023) focuses on perturbations against the latent encoder of the LDM. Mist (Liang & Wu, 2023) combines latent and denoising losses in perturbation generation, while AntiDreamBooth (Van Le et al., 2023) creates protective perturbations against the DreamBooth (Ruiz et al., 2023) customization approach. MetaCloak (Liu et al., 2024) leverages a meta-learning framework with transformation sampling to generate transferable and robust perturbations.

Purification-based adaptive attacks have recently been proposed against existing protection methods. IMPRESS (Cao et al., 2024) introduces a purification technique that minimizes the difference between the protected image and its reconstruction from the latent autoencoder of the LDM. GrID-Pure (Zhao et al., 2024) builds upon DiffPure (Nie et al., 2022) to pre-process protected samples. Additionally, the authors in (Hönig et al., 2024) propose using Noisy-Upscaling to purify protected image samples before customization. However, all these methods decrease the effectiveness of protective perturbations by purifying the protected images. To the best of our knowledge, we are the first to address the robustness of protection perturbations in the customization of LDMs from the novel perspective of model adaptation.

3. Understanding Protective Perturbations

3.1. Distortion in Latent Representations

We first identify a key reason why adversarial examples serve as effective protective perturbations in LDMs: their representations are distorted in the latent space. As illustrated in Figure 2, the latent autoencoder of a LDM first encodes a given clean image x_c from pixel space into a latent representation z_c . Subsequently, the denoising module takes the latent representation as input because it has significantly lower dimensionality while still preserving the semantic features. Additionally, it requires that the autoencoder can correctly decode the latent representation z_c back to pixel space, ensuring that the reconstructed image \tilde{x}_c matches the original image x_c in the ideal case. However, the mappings between pixel and latent space are distorted for adversarial examples. For an adversarial example x_a within a perturbation budget δ , the latent representation \hat{z}_a should remain close to z_c within a distance δ_z and correctly

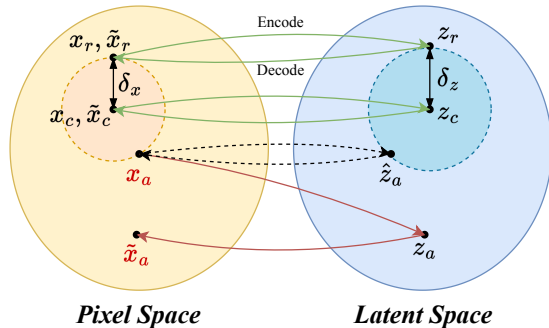


Figure 2. Distortion of latent representations for protected image samples in LDMs. Given a clean image x_c , it is encoded into a latent representation z_c and decoded back to pixel space as \tilde{x}_c . For the protected image x_a , the latent representation \hat{z}_a is distorted, leading to a reconstructed image \tilde{x}_a that deviates significantly from x_a , resulting in a larger reconstruction error.

decode back to x_a in pixel space in the ideal case. However, x_a is instead mapped to a distorted latent representation z_a . This distorted representation is decoded to \tilde{x}_a , which exhibits a significantly larger reconstruction error.

Similar observations about the latent representation are also reported in previous works (Xue et al., 2023; Cao et al., 2024). In contrast, our study conducts more extensive qualitative and quantitative experiments to thoroughly validate the distortion in latent representations of protected samples. To illustrate this, we use t-SNE to visualize the latent representations of various protected samples, as shown in Figure 3. We use four clean images of an identity from the VGGFace2 (Cao et al., 2018) dataset as an illustration. For each clean sample x_c , we generate its adversarial example x_a as the protected image using nine different protective perturbation methods, within the perturbation budget fixed at $\delta = 16/255$. The protected sample is then encoded into the latent space through the latent encoder as $z_a = \mathcal{E}(x_a)$, while the clean sample is encoded as $z_c = \mathcal{E}(x_c)$. Additionally, we construct a noisy sample $x_r = x_c + \text{clip}(r, \delta)$ by adding Gaussian noise $r \sim N(0, \delta^2)$, clipped using the same perturbation budget δ . This noisy sample is encoded as $z_r = \mathcal{E}(x_r)$. Finally, the adversarial sample x_a is also encoded using the latent encoder with the CAT adapter (in the CAT-both setting), resulting in $z_a^{(\text{cat})} = \mathcal{E}^{(\text{cat})}(x_a)$. For each protection method shown in the subplots, z_a , z_r and $z_a^{(\text{cat})}$ are clustered with their corresponding clean sample z_c . Since four images are evaluated for each protection method, their latent representations naturally form four distinct groups. Within each group, it can be observed that the latent representation of the protected sample z_a exhibits a larger distance from the clean sample’s latent representation

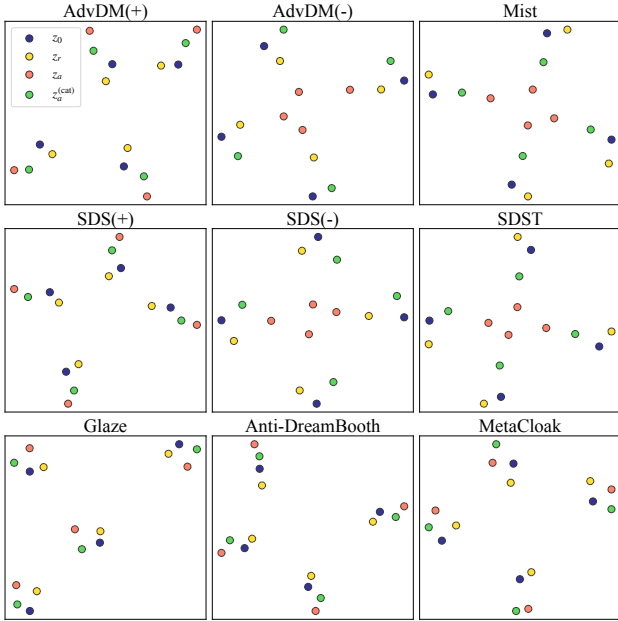


Figure 3. Visualization of latent representations of clean sample z_c , noisy sample z_r , protected sample z_a , and the latent representation of protected sample $z_a^{(\text{cat})}$ encoded by the latent encoder with CAT adapter. Protected samples are generated using nine protective perturbation methods, with four clean images from the VGGFace2 dataset as the base. The perturbation budget for protected and noisy samples is fixed at $\delta = 16/255$.

z_c compared to the noisy sample z_r under the same perturbation budget. This pattern holds across all four image samples for every protective perturbation method, indicating that the latent representations of adversarial examples as protected samples are distorted across all evaluated protection methods. In addition to the qualitative experiments, we provide a quantitative analysis of the distances of latent representations. We define the MAE distance between the latent representation of a sample and its corresponding clean sample as d . Specifically, the distance between z_a and its corresponding z_c is denoted as $d_a = \|z_a - z_c\|_1$, while the distance between $z_a^{(\text{cat})}$ and its corresponding z_c is represented as $d_a^{(\text{cat})} = \|z_a^{(\text{cat})} - z_c\|_1$. The distance between a noisy sample z_r and its corresponding z_c is denoted as $d_r = \|z_r - z_c\|_1$. For comparison, we present the differences between d_a and $d_a^{(\text{cat})}$ over d_r , as shown in Figure 4. As we can observe, d_a is larger than d_r across all the evaluated protection methods, indicating that adversarial examples significantly distort their latent representations compared to noisy samples with the same perturbation budget. Furthermore, our proposed CAT adapter method can effectively reduce this distortion, realigning the latent representations of protected examples closer to their correct

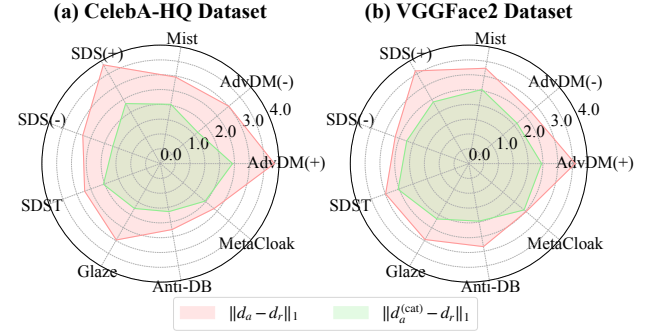


Figure 4. Comparison of latent representation distances $\|d_a - d_r\|$ and $\|d_a^{(\text{cat})} - d_r\|$ for various protective perturbation methods across (a) CelebA-HQ and (b) VGGFace2 datasets. The mean distance values over four images for each method are presented, highlighting the CAT adapter’s effectiveness in reducing latent representation distortion.

positions.

3.2. Learnability of Distorted Latent Representations

We have identified that a key reason for the effectiveness of adversarial examples as protective perturbations is the distortion of their latent representations. Building on this finding, we seek to explore a further question: Can the latent representations of adversarial examples be effectively learned by the diffusion process?

To explore this, we design the following experiment: diffusion models are known to overfit when trained or fine-tuned on a very small number of image samples. In such cases, the overfitted model exhibits memorization, generating samples nearly identical to the training images when given the same text prompts used during fine-tuning. We first fine-tune the pre-trained LDM on a single image obtained from one identity in the dataset. Once the model overfits, we generate an image from the fine-tuned model using the exact same text prompt. For the latent representation z_c of a clean image, we expect the generated \tilde{z}_c to be close to z_c in the latent space. The difference ratio for this clean image is defined as $s_c = \|z_c - \tilde{z}_c\|/z_b$, where $z_b = \max(z_c) - \min(z_c)$ serves as a normalization term. Subsequently, the difference ratios for s_r , s_a and $s_a^{(\text{cat})}$ are defined as $\|z_r - \tilde{z}_c\|/z_b$, $\|z_a - \tilde{z}_c\|/z_b$ and $\|z_a^{(\text{cat})} - \tilde{z}_c\|/z_b$, respectively. For simplicity, we also define the s_r range as $[s_c - \|s_c - s_r\|, s_c + \|s_c - s_r\|]$. We present the evaluation results in Figure 5. The difference ratios are evaluated for nine protection methods based on the sample clean image from an identity in the VGGFace2 dataset and two fine-tuning approaches, DreamBooth and LoRA. As shown in Figure 5, s_a consistently falls within or near the range of $s_c \pm s_r$ across all protection methods and both fine-tuning approaches, which suggests that the

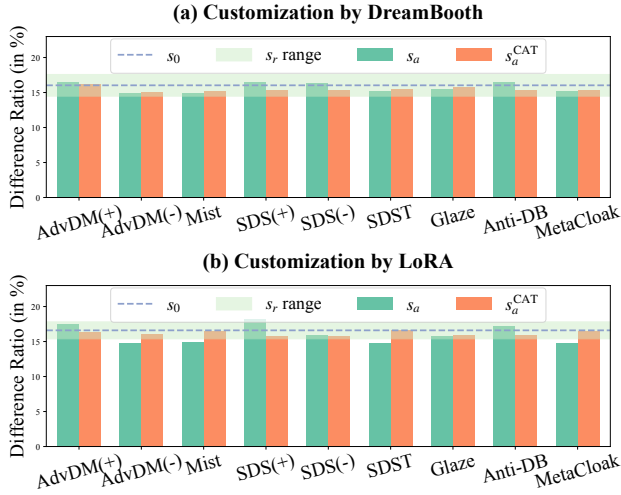


Figure 5. Difference ratios for nine protection methods, evaluated using an image from the VGGFace2 dataset. Results are shown for two fine-tuning approaches: (a) by DreamBooth and (b) by LoRA. The s_r range $[s_c - \|s_c - s_r\|, s_c + \|s_c - s_r\|]$ is shaded, demonstrating that s_a consistently falls within or near this range across all methods, indicating that both clean samples and adversarial examples can be effectively learned by the diffusion process.

latent representations of both clean samples and adversarial examples can be effectively learned by the diffusion process. This indicates that the primary reason for the effectiveness of adversarial examples as protective perturbation methods lies in the distortion of their latent representations, rather than the limitation of the diffusion process in learning these distorted representations.

In summary, this section provides a deeper investigation into why adversarial examples of LDMs are effective as protective perturbations against unauthorized data usage. We identify that the primary reason lies in the distortion of latent representations for these adversarial examples. Furthermore, we verify that these distorted latent representations can still be effectively learned by the diffusion process, confirming that the distortion itself is the key factor behind their effectiveness.

4. CAT: Contrastive Adversarial Training

4.1. Contrastive Adversarial Loss

We have observed that adversarial examples are effective as protective perturbations because their latent representations are distorted. This indicates that the latent autoencoder $\{\mathcal{E}_\phi, \mathcal{D}_\omega\}$ of the LDM is attacked. To mitigate this, we apply contrastive adversarial training to the latent autoencoder to realign the latent representations of adversarial examples. We first introduce the contrastive adversarial loss used for

contrastive adversarial training as follows. Given the protected image x_a and the latent autoencoder $\{\mathcal{E}_\phi, \mathcal{D}_\omega\}$, we define the loss function as

$$\mathcal{L}_{\text{cat}}(\mathcal{E}_\phi, \mathcal{D}_\omega, x_a) = \mathbb{E}_{x_a} \|\mathcal{D}_\omega(\mathcal{E}_\phi(x_a)) - x_a\|_2^2. \quad (1)$$

The protected image is first encoded into the latent space by the encoder \mathcal{E}_ϕ and then decoded back into the pixel space by \mathcal{D}_ω . Since the decoded image should ideally match the original protected image, we define the contrastive loss as the MSE distance between them over all given x_a . This loss encourages the autoencoder to correctly reconstruct x_a , restoring its latent representation.

4.2. CAT Adapters

Fine-tuning all layers of the latent autoencoder may affect the model’s performance in encoding and decoding unprotected image samples. Moreover, we aim to introduce additional parameters to expand the parameter space, improving the model’s resilience against adversarial examples after the contrastive adversarial training. Therefore, we incorporate adapters in our proposed contrastive adversarial training. Specifically, we apply the LoRA (Hu et al., 2022) adapter to all convolutional and attention layers within the latent autoencoder. For the model weights $\phi_0 \in \mathbb{R}^{d \times k}$ of the latent encoder, the latent representation $z_a^{(\text{cat})}$ of a protected sample x_a is given by

$$z_a^{(\text{cat})} = \phi_0 x_a + \Delta \phi x_a = \phi_0 x_a + B^\phi A^\phi x_a, \quad (2)$$

where $B^\phi \in \mathbb{R}^{d \times r}$ and $A^\phi \in \mathbb{R}^{r \times k}$ are the weights of the CAT adapter attached to the latent encoder.

Similarly, for the model weights $\omega_0 \in \mathbb{R}^{k \times d}$ of the latent decoder, the reconstruction $\hat{x}_a^{(\text{cat})}$ in pixel space of the latent representation $z_a^{(\text{cat})}$ is given by

$$\begin{aligned} \hat{x}_a^{(\text{cat})} &= \omega_0 z_a^{(\text{cat})} + \Delta \omega z_a^{(\text{cat})} \\ &= \omega_0 z_a^{(\text{cat})} + B^\omega A^\omega z_a^{(\text{cat})}, \end{aligned} \quad (3)$$

where $B^\omega \in \mathbb{R}^{k \times r}$ and $A^\omega \in \mathbb{R}^{r \times d}$ are the weights of the CAT adapter attached to the latent decoder. The overall design of our proposed CAT method is illustrated in Figure 1. For a protected image sample x_a , we do not directly use its encoded latent representation z_a for the denoising module to learn in the diffusion process. Instead, we first apply CAT by encoding x_a using the latent encoder attached with the CAT adapter $\Delta \phi$, obtaining the realigned latent representation $z_a^{(\text{cat})}$. This realigned representation is then decoded back using the latent decoder, which is also attached with the CAT adapter $\Delta \omega$, resulting in the reconstructed image $\hat{x}_a^{(\text{cat})}$ in the pixel space. Our proposed CAT method is optimized by solving the following objective:

$$\Delta \phi, \Delta \omega = \arg_{\Delta \phi, \Delta \omega} \min \mathcal{L}_{\text{cat}}(\mathcal{E}_\phi^{\text{cat}}, \mathcal{D}_\omega^{\text{cat}}, x_a), \quad (4)$$

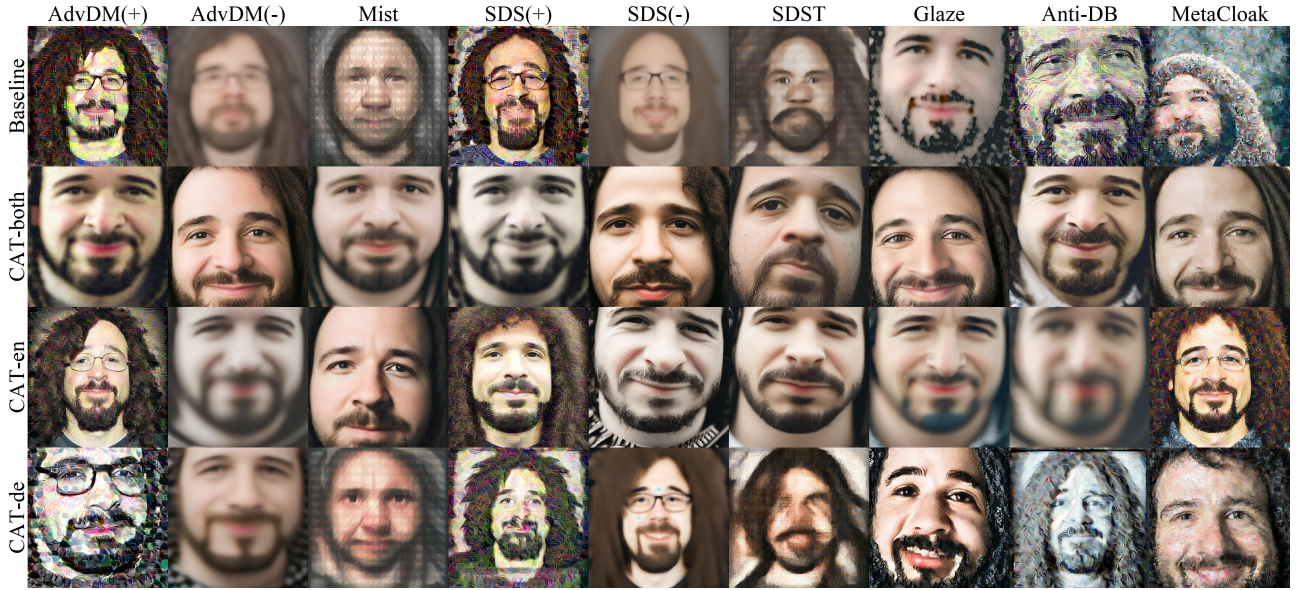


Figure 6. Qualitative results for object-driven image synthesis customization in an identity from the VGGFace2 dataset using DreamBooth and CAT settings with the text prompt ”a dslr portrait of *sks* person”. Each row represents a different setting: Baseline, CAT-both, CAT-en, and CAT-de, while each column corresponds to a different protective perturbation setting. The results illustrate the effectiveness of different CAT settings on generating human faces from protected images.

where the weights for model $\mathcal{E}_\phi^{\text{cat}}$ are $\phi_0 + \Delta\phi$ and the weights for model $\mathcal{D}_\omega^{\text{cat}}$ are $\omega_0 + \Delta\omega$.

Once CAT is applied and the CAT adapters are obtained, customization on protected image samples is performed using the latent autoencoder augmented with the CAT adapters. For image generation, since the denoising module is fine-tuned on the realigned latent representation $z_a^{(\text{cat})}$, the generated output in the latent space for a given prompt is also realigned. Consequently, it is decoded into the image $\tilde{x}_a^{(\text{cat})}$ in the pixel space instead of \tilde{x}_a , effectively neutralizing the protective perturbations.

5. Experiments

5.1. Experimental Setup

Evaluated Protective Perturbation Methods To evaluate the effectiveness of our proposed CAT method in compromising the robustness of protective perturbations, we test CAT across nine protective perturbation settings: (1) AdvDM(+) (Liang et al., 2023), (2) AdvDM(-) (Xue et al., 2023), (3) Mist (Liang & Wu, 2023), (4) SDS(+) (Xue et al., 2023), (5) SDS(-) (Xue et al., 2023), (6) SDST (Xue et al., 2023), (7) Glaze (Shan et al., 2023), (8) Anti-DreamBooth (Van Le et al., 2023), and (9) MetaCloak (Liu et al., 2024). The (+) sign denotes the use of gradient ascent to construct the perturbation, whereas the (-) sign denotes the use of gradient descent, following the setting in (Xue

et al., 2023). We set the perturbation budget for all evaluated protection methods to $\delta = 16/255$. Since Glaze does not release its codebase and its application does not allow adjustment of the specific perturbation budget, we use its maximum perturbation strength.

Datasets We evaluate the effectiveness of CAT in two main diffusion-based image synthesis applications: (1) object-driven image synthesis and (2) style mimicry. Object-driven image synthesis focuses on generating images of a specific object based on a given text prompt, such as the face of a particular person or a photo of a specific dog. Style mimicry, conversely, aims to generate images that mimic the style of the provided customization images.

For object-driven image synthesis, we focus on human face generation using the CelebA-HQ (Karras et al., 2018) and VGGFace2 (Cao et al., 2018) datasets. For each dataset, we select five identities, with 12 images per identity, equally split into three subsets: a clean reference subset, a target protection subset, and an additional clean reference subset. For style mimicry, due to page constraints, we present only qualitative results to demonstrate the effectiveness of CAT. We use a subset of *Claude Monet’s* artworks from the WikiArt dataset (Mancini et al., 2018), consisting of 12 images, divided into three subsets following the same configuration. All images are center-cropped and resized to 512×512 .

CAT Settings For object-driven image synthesis, we evalu-

Table 1. Quantitative results for object-driven image synthesis using CAT methods customized in DreamBooth. The table presents performance metrics FSS and FQS for the CelebA-HQ and VGGFace2 datasets across different protective perturbation settings. The optimal values among different CAT settings for each metric are **bolded**, where higher FSS indicates improved human face similarity, and higher FQS reflects better face image quality.

DATASET	CELEBA-HQ								VGGFACE2							
	FSS \uparrow				FQS \uparrow				FSS \uparrow				FQS \uparrow			
METHOD	BASELINE	CAT-BOTH	CAT-EN	CAT-DE	BASELINE	CAT-BOTH	CAT-EN	CAT-DE	BASELINE	CAT-BOTH	CAT-EN	CAT-DE	BASELINE	CAT-BOTH	CAT-EN	CAT-DE
AdvDM(+)	0.340	0.643	0.529	0.344	0.244	0.431	0.448	0.340	0.390	0.534	0.560	0.416	0.257	0.460	0.600	0.331
AdvDM(-)	0.354	0.623	0.571	0.401	0.275	0.549	0.611	0.401	0.436	0.564	0.547	0.454	0.281	0.617	0.662	0.492
MIST	0.160	0.572	0.501	0.152	0.286	0.597	0.580	0.375	0.035	0.557	0.521	0.101	0.384	0.656	0.712	0.279
SDS(+)	0.352	0.602	0.499	0.342	0.282	0.413	0.423	0.399	0.397	0.486	0.508	0.305	0.406	0.502	0.532	0.410
SDS(-)	0.411	0.678	0.599	0.405	0.352	0.597	0.587	0.449	0.439	0.570	0.569	0.435	0.368	0.730	0.689	0.456
SDST	0.175	0.594	0.485	0.157	0.208	0.587	0.588	0.313	0.146	0.559	0.546	0.196	0.248	0.663	0.694	0.346
GLAZE	0.363	0.610	0.577	0.398	0.491	0.618	0.676	0.587	0.387	0.607	0.576	0.472	0.576	0.724	0.740	0.595
ANTI-DB	0.471	0.662	0.597	0.489	0.434	0.608	0.664	0.546	0.456	0.584	0.546	0.440	0.416	0.673	0.704	0.401
METACLOAK	0.497	0.642	0.578	0.507	0.372	0.460	0.475	0.403	0.421	0.560	0.631	0.487	0.355	0.508	0.625	0.412

ate three CAT settings: (1) CAT-both, (2) CAT-en, and (3) CAT-de. In CAT-both, CAT adapters are added to the target layers in both the encoder and decoder of the latent autoencoder. CAT-en applies CAT adapters only to the encoder, while CAT-de applies them solely to the decoder. Since we have identified that the primary reason adversarial examples are effective as protective perturbations is their latent representation distortion, the CAT-de method should have no impact on compromising the protection. We conduct this evaluation to verify our hypothesis. For style mimicry, we only evaluate (1) CAT-both, and (2) CAT-en settings.

We select all convolutional and attention layers within the module as the target layers. The adapter rank is set to $r = 128$ for the CAT-both setting and $r = 256$ for the CAT-en and CAT-de settings to maintain the same number of parameters. During CAT, only the weights of the attached adapters are updated, while all other weights remain frozen. Training is performed with a batch size of 4 and a learning rate of 1×10^{-4} for 1000 steps.

Customization Settings For the customization settings, we adopt the widely used DreamBooth (Ruiz et al., 2023) and LoRA (Hu et al., 2022) methods, using the latest Stable Diffusion v2.1 as the pre-trained LDM. Details of the customization settings are provided in Appendix B.

Evaluation Metrics For Qualitative Experiments The object-driven image synthesis task aims to generate human faces that preserve the identity features from the given protected images. Therefore, for qualitative experiments, we use Face Detection Rate (Retina-FDR), measured with the RetinaFace detector (Deng et al., 2020), to evaluate whether a face is detected in the generated images. If a face is detected, we extract its embedding using the ArcFace recognizer (Deng et al., 2019) and compute the cosine distance between the extracted embedding and those from the clean dataset, denoted as Identity Score Matching (ISM). To quantify the expected identity similarity in the generated image

set, we define Face Similarity Score (FSS) as the product of Retina-FDR and ISM.

Moreover, we employ the TOPIQ method (Chen et al., 2024), trained on the face IQA dataset and implemented in (Chen & Mo, 2022), to measure Face Detection Rate (TOPIQ-FDR) and Face Image Quality (FIQ). To quantify the expected quality of the generated face images, we define their product as the Face Quality Score (FQS). We use two text prompts for sampling, "a photo of *sks* person" and "a dsr portrait of *sks* person". For each test prompt, we generate 30 images and compute the average metric scores across all tested identities to obtain the final results.

5.2. Object-driven Synthesis Results

The evaluation results for applying CAT methods in the object-driven image synthesis task are presented in Table 1. We observe that both the CAT-both and CAT-en settings significantly improve task performance compared to the baseline, which directly customizes using the protected image samples across all evaluated protections. This demonstrates the effectiveness of these two settings in compromising the protective perturbations. Furthermore, the CAT-both setting achieves a higher FSS score than CAT-en, while CAT-en obtains a better FQS score overall. Additionally, the CAT-de setting has little to no effect on improving task performance, further verifying that the primary reason adversarial examples function effectively as protective perturbations is their latent representation distortion. Qualitative results for the identity *n000050* from the VGGFace2 dataset, as shown in Figure 6 (for the identity 5 from the CelebA-HQ dataset in Appendix A.1), further confirm the observations from the quantitative results. Moreover, we also experimented with object-driven image synthesis customization using LoRA, as shown in Appendix A.2. The results verify the effectiveness of CAT in the LoRA customization setting across all nine evaluated protective perturbations and two datasets.

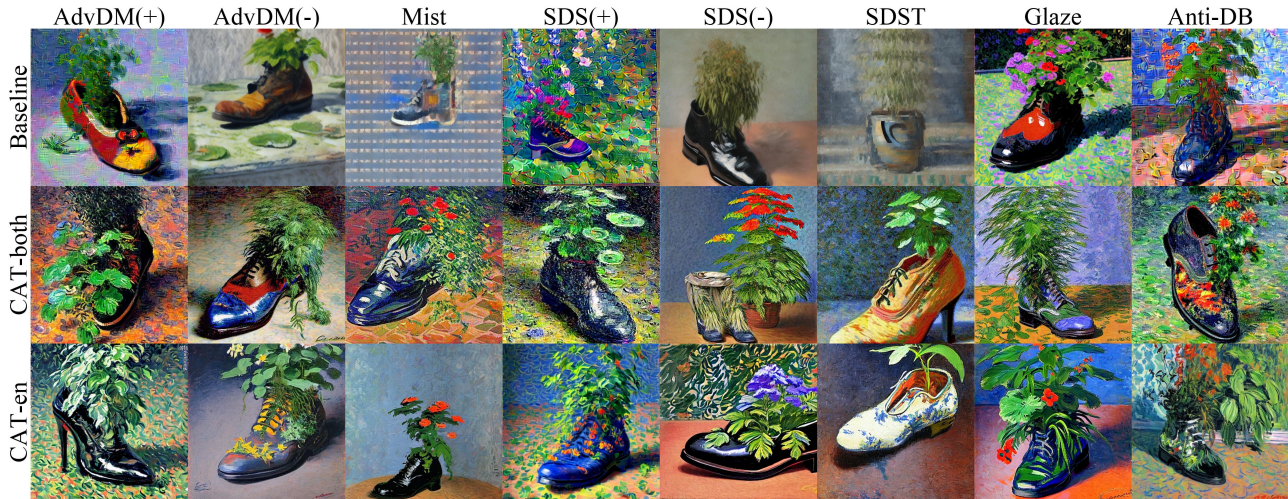


Figure 7. Qualitative results for style mimicry customization in DreamBooth using CAT settings with the text prompt ”a painting of shoe with a plant growing inside by *claudesimonet* artist”. Each row represents a different setting: Baseline, CAT-both and CAT-en, while each column corresponds to a different protective perturbation setting. The results illustrate the effectiveness of different CAT settings on generating artworks of the same style from protected images.

5.3. Style Mimicry Results

We evaluate only the CAT-both and CAT-en settings for style mimicry customization using DreamBooth to verify their effectiveness in compromising the protective perturbations. Qualitative results are presented in Figure 7, demonstrating that applying CAT leads to a significant improvement in the task performance of style mimicry customization. Across all evaluated protective perturbations, applying CAT preserves the specific artist’s style and improves the fidelity of generated images while reducing the distortions introduced by the protections. These results demonstrate that CAT weakens the robustness of existing protective perturbations, enabling more precise style mimicry and highlighting the need for more effective defense mechanisms.

5.4. Ablation Study: Impact of CAT Adapter Rank

To investigate the impact of the CAT adapter rank on the effectiveness, we conduct experiments using different rank settings on the VGGFace2 dataset under the AdvDM(+) protective perturbation and CAT-both setting. The results shown in Table 2 indicate that increasing the rank generally improves performance, with $r = 128$ achieving the highest FSS (0.544) and FQS (0.460). This demonstrates that higher-rank adapters enhance robustness against protective perturbations.

However, higher-rank CAT adapters result in a larger model size. For instance, the CAT-both setting with $r = 128$ produces a 104 MB adapter model, and this size continues to grow with increasing rank. This trade-off suggests

that while higher-rank adapters enhance robustness against protective perturbations, practical deployment requires balancing performance gains and model efficiency.

Table 2. Effectiveness of the CAT-both method against AdvDM(+) protective perturbation on the VGGFace2 dataset at various CAT adapter rank settings for human face generation using DreamBooth. The optimal values for each metric are highlighted in **bold**.

RANK	BASELINE	$r = 4$	$r = 8$	$r = 16$	$r = 32$	$r = 64$	$r = 128$
FSS \uparrow	0.350	0.525	0.500	0.513	0.489	0.540	0.544
FQS \uparrow	0.260	0.372	0.390	0.458	0.414	0.381	0.460

6. Conclusions

In conclusion, we introduce contrastive adversarial training as a novel approach to evaluating the robustness of LDM customization against protective perturbations. We first reveal that the primary reason adversarial examples serve as effective protective perturbations in LDM customization is the distortion of their latent representation. We then propose CAT, which employs adapters in adversarial training by leveraging contrastive adversarial loss. Extensive experiments demonstrate that CAT significantly decreases the effectiveness of existing protective perturbations. We believe this work can remind the community to reconsider the robustness of current protective perturbation methods.

References

- Cao, B., Li, C., Wang, T., Jia, J., Li, B., and Chen, J. Impress: Evaluating the resilience of imperceptible perturbations against unauthorized data usage in diffusion-based generative ai. *Advances in Neural Information Processing Systems*, 36, 2024.
- Cao, Q., Shen, L., Xie, W., Parkhi, O. M., and Zisserman, A. Vggface2: A dataset for recognising faces across pose and age. In *2018 13th IEEE international conference on automatic face & gesture recognition (FG 2018)*, pp. 67–74. IEEE, 2018.
- Chen, C. and Mo, J. IQA-PyTorch: Pytorch toolbox for image quality assessment. [Online]. Available: <https://github.com/chaofengc/IQA-PyTorch>, 2022.
- Chen, C., Mo, J., Hou, J., Wu, H., Liao, L., Sun, W., Yan, Q., and Lin, W. Topiq: A top-down approach from semantics to distortions for image quality assessment. *IEEE Transactions on Image Processing*, 2024.
- Deng, J., Guo, J., Xue, N., and Zafeiriou, S. Arcface: Additive angular margin loss for deep face recognition. In *Proceedings of the IEEE/CVF conference on computer vision and pattern recognition*, pp. 4690–4699, 2019.
- Deng, J., Guo, J., Verweras, E., Kotsia, I., and Zafeiriou, S. Retinaface: Single-shot multi-level face localisation in the wild. In *Proceedings of the IEEE/CVF conference on computer vision and pattern recognition*, pp. 5203–5212, 2020.
- Dhariwal, P. and Nichol, A. Diffusion models beat gans on image synthesis. *Advances in neural information processing systems*, 34:8780–8794, 2021.
- Dixit, P. Meet the three artists behind a landmark lawsuit against ai art generators. *Buzzfeed News*, 2023.
- Goodfellow, I. J., Shlens, J., and Szegedy, C. Explaining and harnessing adversarial examples. *arXiv preprint arXiv:1412.6572*, 2014.
- Ho, J., Jain, A., and Abbeel, P. Denoising diffusion probabilistic models. *Advances in neural information processing systems*, 33:6840–6851, 2020.
- Hönig, R., Rando, J., Carlini, N., and Tramèr, F. Adversarial perturbations cannot reliably protect artists from generative ai. *arXiv preprint arXiv:2406.12027*, 2024.
- Hu, E. J., Wallis, P., Allen-Zhu, Z., Li, Y., Wang, S., Wang, L., Chen, W., et al. Lora: Low-rank adaptation of large language models. In *International Conference on Learning Representations*, 2022.
- Karras, T., Aila, T., Laine, S., and Lehtinen, J. Progressive growing of gans for improved quality, stability, and variation. In *International Conference on Learning Representations*, 2018.
- Kawar, B., Zada, S., Lang, O., Tov, O., Chang, H., Dekel, T., Mosseri, I., and Irani, M. Imagic: Text-based real image editing with diffusion models. In *Proceedings of the IEEE/CVF Conference on Computer Vision and Pattern Recognition*, pp. 6007–6017, 2023.
- Li, C., Wang, L., Ji, S., Zhang, X., Xi, Z., Guo, S., and Wang, T. Seeing is living? rethinking the security of facial liveness verification in the deepfake era. In *31st USENIX Security Symposium (USENIX Security 22)*, pp. 2673–2690, 2022.
- Liang, C. and Wu, X. Mist: Towards improved adversarial examples for diffusion models. *arXiv preprint arXiv:2305.12683*, 2023.
- Liang, C., Wu, X., Hua, Y., Zhang, J., Xue, Y., Song, T., Xue, Z., Ma, R., and Guan, H. Adversarial example does good: preventing painting imitation from diffusion models via adversarial examples. In *Proceedings of the 40th International Conference on Machine Learning*, pp. 20763–20786, 2023.
- Liu, Y., Fan, C., Dai, Y., Chen, X., Zhou, P., and Sun, L. Metacloak: Preventing unauthorized subject-driven text-to-image diffusion-based synthesis via meta-learning. In *Proceedings of the IEEE/CVF Conference on Computer Vision and Pattern Recognition*, pp. 24219–24228, 2024.
- LLP, J. S. L. F. Class action filed against stability ai, mid-journey, and deviantart for dmca violations, right of publicity violations, unlawful competition, breach of tos. *PR Newswire*, 2023.
- Lugmayr, A., Danelljan, M., Romero, A., Yu, F., Timofte, R., and Van Gool, L. Repaint: Inpainting using denoising diffusion probabilistic models. In *Proceedings of the IEEE/CVF conference on computer vision and pattern recognition*, pp. 11461–11471, 2022.
- Mancini, M., Ricci, E., Caputo, B., and Rota Bulò, S. Adding new tasks to a single network with weight transformations using binary masks. In *Proceedings of the European Conference on Computer Vision (ECCV) Workshops*, pp. 0–0, 2018.
- Meng, C., He, Y., Song, Y., Song, J., Wu, J., Zhu, J.-Y., and Ermon, S. Sedit: Guided image synthesis and editing with stochastic differential equations. In *International Conference on Learning Representations*, 2021.

- Nie, W., Guo, B., Huang, Y., Xiao, C., Vahdat, A., and Anandkumar, A. Diffusion models for adversarial purification. In *International Conference on Machine Learning*, pp. 16805–16827. PMLR, 2022.
- Rombach, R., Blattmann, A., Lorenz, D., Esser, P., and Ommer, B. High-resolution image synthesis with latent diffusion models. In *Proceedings of the IEEE/CVF conference on computer vision and pattern recognition*, pp. 10684–10695, 2022.
- Ronneberger, O., Fischer, P., and Brox, T. U-net: Convolutional networks for biomedical image segmentation. In *Medical image computing and computer-assisted intervention—MICCAI 2015: 18th international conference, Munich, Germany, October 5-9, 2015, proceedings, part III 18*, pp. 234–241. Springer, 2015.
- Ruiz, N., Li, Y., Jampani, V., Pritch, Y., Rubinstein, M., and Aberman, K. Dreambooth: Fine tuning text-to-image diffusion models for subject-driven generation. In *Proceedings of the IEEE/CVF conference on computer vision and pattern recognition*, pp. 22500–22510, 2023.
- Saharia, C., Chan, W., Chang, H., Lee, C., Ho, J., Salimans, T., Fleet, D., and Norouzi, M. Palette: Image-to-image diffusion models. In *ACM SIGGRAPH 2022 conference proceedings*, pp. 1–10, 2022.
- Salman, H., Khaddaj, A., Leclerc, G., Ilyas, A., and Madry, A. Raising the cost of malicious ai-powered image editing. In *Proceedings of the 40th International Conference on Machine Learning*, pp. 29894–29918, 2023.
- Shan, S., Cryan, J., Wenger, E., Zheng, H., Hanocka, R., and Zhao, B. Y. Glaze: Protecting artists from style mimicry by {Text-to-Image} models. In *32nd USENIX Security Symposium (USENIX Security 23)*, pp. 2187–2204, 2023.
- Stability.ai. Stability ai image models — stability ai. <https://stability.ai/stable-image>, 2024. Accessed: 2024-07-25.
- Van Le, T., Phung, H., Nguyen, T. H., Dao, Q., Tran, N. N., and Tran, A. Anti-dreambooth: Protecting users from personalized text-to-image synthesis. In *Proceedings of the IEEE/CVF International Conference on Computer Vision*, pp. 2116–2127, 2023.
- Xue, H., Liang, C., Wu, X., and Chen, Y. Toward effective protection against diffusion-based mimicry through score distillation. In *The Twelfth International Conference on Learning Representations*, 2023.
- Zhang, Y., Huang, N., Tang, F., Huang, H., Ma, C., Dong, W., and Xu, C. Inversion-based style transfer with diffusion models. In *Proceedings of the IEEE/CVF conference on computer vision and pattern recognition*, pp. 10146–10156, 2023.
- Zhao, Z., Duan, J., Xu, K., Wang, C., Zhang, R., Du, Z., Guo, Q., and Hu, X. Can protective perturbation safeguard personal data from being exploited by stable diffusion? In *Proceedings of the IEEE/CVF Conference on Computer Vision and Pattern Recognition*, pp. 24398–24407, 2024.

A. Additional Experimental Results

A.1. Qualitative Results for Object-Driven Image Synthesis in DreamBooth (CelebA-HQ)

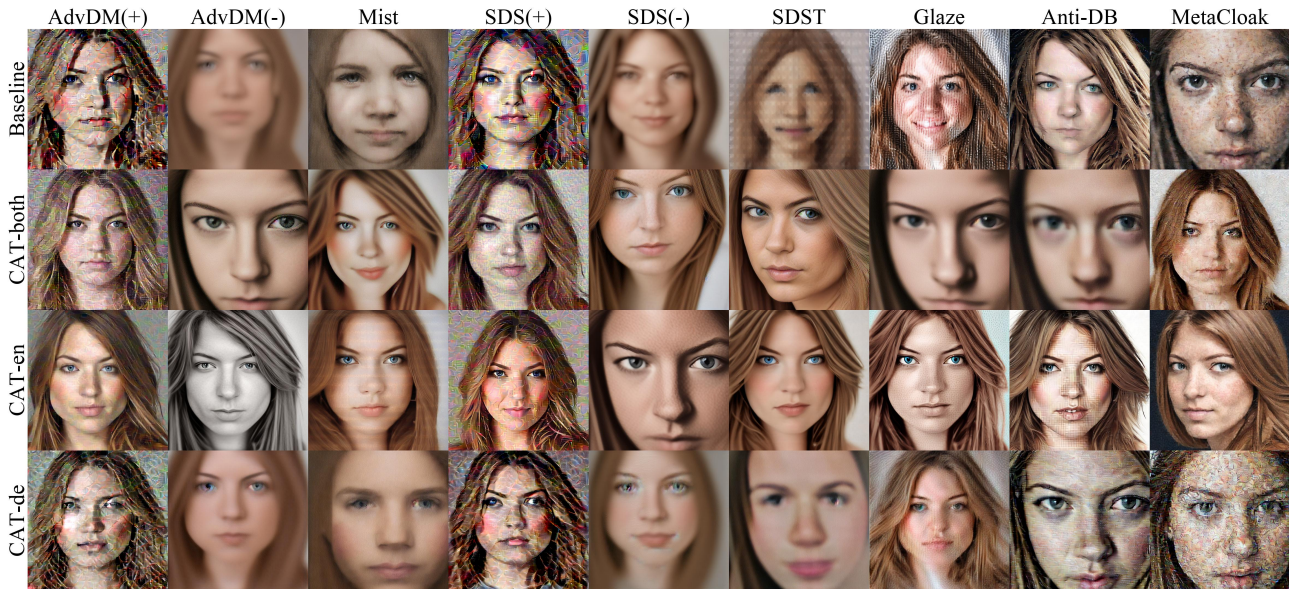


Figure 8. Qualitative results for object-driven image synthesis customization in an identity from the CelebA-HQ dataset using DreamBooth and CAT settings with the text prompt "a dslr portrait of sks person". Each row represents a different setting: Baseline, CAT-both, CAT-en, and CAT-de, while each column corresponds to a different protective perturbation setting. The results illustrate the effectiveness of different CAT settings on generating human faces from protected images.

A.2. Customization for Object-driven Image Synthesis in LoRA

Table 3. Quantitative results for object-driven image synthesis using CAT methods customized in DreamBooth. The table presents performance metrics FSS and FQS for the CelebA-HQ and VGGFace2 datasets across different protective perturbation settings. The optimal values among different CAT settings for each metric are **bolded**.

DATASET	CELEBA-HQ								VGGFACE2							
	FSS \uparrow				FQS \uparrow				FSS \uparrow				FQS \uparrow			
METHOD	BASILINE	CAT-BOTH	CAT-EN	CAT-DE	BASILINE	CAT-BOTH	CAT-EN	CAT-DE	BASILINE	CAT-BOTH	CAT-EN	CAT-DE	BASILINE	CAT-BOTH	CAT-EN	CAT-DE
ADVDM+	0.351	0.574	0.455	0.402	0.260	0.369	0.585	0.377	0.301	0.490	0.417	0.377	0.257	0.400	0.499	0.404
ADVDM-	0.424	0.653	0.608	0.505	0.235	0.568	0.686	0.480	0.367	0.616	0.598	0.482	0.281	0.593	0.729	0.409
MIST	0.135	0.565	0.516	0.005	0.363	0.469	0.532	0.022	0.069	0.596	0.476	0.001	0.384	0.565	0.706	0.000
SDS+	0.464	0.497	0.559	0.285	0.381	0.328	0.525	0.389	0.393	0.541	0.443	0.413	0.406	0.399	0.505	0.392
SDS-	0.476	0.625	0.586	0.535	0.297	0.583	0.665	0.490	0.353	0.620	0.591	0.480	0.368	0.633	0.695	0.416
SDST5	0.203	0.572	0.486	0.032	0.217	0.488	0.574	0.137	0.112	0.549	0.544	0.052	0.248	0.578	0.716	0.217
GLAZE2	0.355	0.669	0.575	0.479	0.474	0.714	0.752	0.617	0.330	0.602	0.611	0.472	0.576	0.673	0.755	0.586
ANTIDB	0.539	0.596	0.616	0.465	0.497	0.458	0.541	0.411	0.460	0.583	0.586	0.439	0.416	0.569	0.725	0.494
METACLOAK	0.528	0.597	0.543	0.549	0.376	0.442	0.458	0.444	0.416	0.520	0.513	0.431	0.355	0.531	0.551	0.496

B. Details of Customization Settings

In the DreamBooth customization setting, both the U-Net and text encoder are fine-tuned with a batch size of 2 and a learning rate of 5×10^{-7} for 2000 training steps. The training instance and prior class prompt for object-driven image synthesis are "a photo of sks person" and "a photo of person", respectively. For style mimicry, the training instance and prior class prompt are "a painting by [ARTIST] artist" and "a painting by artist", where [ARTIST] is replaced with the target artist's name. In the LoRA customization setting, LoRA adapters are added only to the U-Net with a rank of 4 and fine-tuned using a batch size of 2 and a learning rate of 5×10^{-5} for 2000 training steps.